Förster, H.-J., Rhede, D., Stein, H. J., Romer, R. L., Tischendorf, G. (2012): Paired uraninite and molybdenite dating of the Königshain granite: implications for the onset of late-Variscan magmatism in the Lausitz Block. - International Journal of Earth Sciences, 101, 1, 57-67

DOI: 10.1007/s00531-010-0631-1

# Paired uraninite and molybdenite dating of the Königshain granite: implications for the onset of late-Variscan magmatism in the Lausitz Block

**Hans-Jürgen Förster, Dieter Rhede, Holly J. Stein, Rolf L. Romer, Gerhard Tischendorf**

## Abstract

We present geochronological data for late-Variscan magmatism in the Lausitz Block of the Saxo-Thuringian Zone, Germany. The Th–U–total Pb age of uraninite and the Re–Os age of molybdenite from the composite biotite-monzogranite pluton of Königshain overlap at the 2σ confidence limit: 328.6 ± 1.9 Ma (uraninite) and 327.0 ± 1.3 Ma and 327.6 ± 1.3 Ma (molybdenite), indicating that crystallization of magmatic uraninite and deposition of molybdenite were nearly contemporaneous. These data imply that magmatic processes in this part of the Variscan orogen already started in latest Visean time, about 10 Ma earlier than previously assumed (315–320 Ma). The new ages correspond to ages for plutonic rocks in the Elbe Zone immediately west of the Lausitz (around 335–325 Ma) and the bulk of late-Variscan igneous rocks in the Saxo-Thuringian Zone (335–320 Ma).

**Keywords** U–Th–total Pb, Re–Os, uraninite, molybdenite, Variscan, Königshain, Lausitz, Saxo-Thuringia

## Introduction

The Saxo-Thuringian Zone of the Variscan Orogen consists mainly of a Cadomian basement and its overlying volcano-sedimentary cover. It is divided into three structurally different segments based on Variscan overprint, the Autochthonous Domain, the Allochthonous Domain, and the Wrench–and–Thrust Zone separating them (Fig. 1) The Autochthonous Domain largely escaped deformation and metamorphism during the Variscan orogeny, whereas the Allochthonous Domain consists of the metamorphic complexes of the Saxon

Granulite Massif and the metamorphic nappes of the Erzgebirge–Vogtland Zone (Kroner et al. 2007, 2010). To the SE, the bipartite Wrench–and–Thrust Zone consists of the same rocks as the Autochthonous Domain, but differs from the former in that late-Variscan folding of the sediments took place, including clastic sediments derived from the evolving Variscan Orogen (cf. Kroner et al. 2007; Hahn et al. 2010)

The Lausitz Block (LB) is the largest exposure of rocks of the Autochthonous Domain (Figs. 1 and 2). Late-Variscan igneous rocks in the LB are poorly exposed and volumetrically minor in comparison to granodiorites and graywackes constituting the Cadomian basement. Variscan granitoids are amphibole- and biotite-bearing. The most prominent of the biotite(±muscovite)-bearing plutons is the reversely zoned massif of Königshain/Arnsdorf (Eidam and Götze 1991; Hecht et al. 1999). Other members of this granite group are the monzogranites of Stolpen and Kleinnaundorf and the granodiorites from Oberprauske and Brösnitz (Fig. 2a; Hammer 1996).

Ages for Variscan granitoids in the LB are mainly determined from single-zircon evaporation data. $^{207}Pb/^{206}Pb$ zircon ages (2σ) obtained for amphibole-bearing granitoids have large errors and scatter between 304 ± 10 Ma (monzogranite from Wiesa; Kröner et al. 1994) and 312 ± 10 Ma (tonalite from Kleinschweidnitz; Hammer et al. 1999). The Königshain granite has been dated at 315 ± 6 Ma (Hammer et al. 1999). For a miarolitic pegmatite from Königshain, Thomas et al. (2009) obtained a U–Th–total Pb (monazite+xenotime+uraninite) isochron age of ~320 Ma and a mean U–Th–total Pb zircon age of 322 Ma (± 30 Ma, 1σ). Hammer et al. (1999) concluded that granite-forming processes in the LB took place between 305 and 315 Ma. The implication of this conclusion would be that Variscan magmatism in the Lausitz occurred temporally between the two major Variscan igneous events recorded in the Saxo-Thuringian Zone (STZ) and, on the larger scale, the Bohemian Massif (Förster et al. 1999; Finger et al. 2009; Förster and Romer 2010). In the STZ, these events occurred ~335–320 Ma and ~305–(280) Ma (cf. Förster and Romer 2010). The age of microgranite/rhyolite from the Altenberg–Teplice volcanic complex in the Eastern Erzgebirge (previously inferred to be ~313 to 308 Ma on the basis of paleobotanical data on sedimentary rocks occurring together with volcanic rocks; see Ulrych et al. 2006) has been revised to fall into the older group of magmatic rocks of the STZ (Romer et al. 2010). Granites in the Moldanubian part of the Bohemian Massif also show a bimodal age distribution, with voluminously important magmatism at 328–320 Ma Ma and less voluminous magmatism at 310–317 Ma (e.g., Siebel et al. 2003; Finger et al., 2009).

The age of Variscan granites from the Lausitz seems not to fit into this broader context of essentially bi-stadial magmatism in the STZ. To provide additional data for the timing of magmatism in the LB, we selected the granite pluton from Königshain for dating, which contains magmatic and virtually unaltered matrix grains of uraninite and open-space molybdenite crystals. This paper reports and discusses the results of U–Th–total Pb chemical dating of uraninite and $^{187}Re$–$^{187}Os$ dating of molybdenite. Dating of uraninite using the electron-microprobe has provided precise age estimates for several STZ granites (e.g., Förster 1999; Kempe 2003, Romer et al. 2007; Förster et al. 2008, 2009). Re–Os geochronology using molybdenite has been successfully applied in Variscan Europe and elsewhere (e.g., Raith and Stein 2006; Zimmerman et al. 2008).

## Background Information and Sample Locations

The small, late-Variscan granite pluton of Königshain, at the northern edge of the Cadomian Lusatian granodiorite massif (Fig. 2), is composed of three, texturally and geochemically distinct granite varieties, ranging from monzogranite to alkali-feldspar granite (Möbus and Lindert 1967; Eidam and Götze 1991). From outermost to innermost, these are (1) a coarse- to medium-grained, porphyritic granite (~15% of the surface exposure of the pluton), (2) a medium-grained, equigranular, locally porphyritic granite (~80%), and (3) a fine-grained, equigranular granite (~5%).

The granites are Si-rich (74–78 wt% $SiO_2$), weakly peraluminous (A/CNK = 1.03–1.05), poor in $P_2O_5$ (<0.05 wt%), and contain between 400 and 1300 ppm F. Despite their high silica content, the granites are comparatively poor in rare lithophile elements (in ppm) such as Rb (165–440), Cs (5–8), Li (8–45), and Sn (3–9) (Tischendorf et al. 1987; Eidam and Götze 1991; Hammer 1996; Hecht et al. 1999). The more evolved, equigranular granite type, from which the samples for this study were collected, displays affinities with P-poor aluminous A-type granites. Analytical data published by Hecht et al. (1999) reveal a flat chondrite-normalized (CN) $REE_{CN}$ pattern ($La_{CN}/Lu_{CN}$ = 1.25) and a deep negative Eu-anomaly (Eu/Eu* = 0.012) for this textural type. Special features of the Königshain granites are the local occurrence of severely altered rocks, i.e., episyenites (e.g., Hecht et al. 1999), and miarolitic pegmatites containing a broad spectrum of rare Be–Sc–Y–REE–Nb–Bi minerals (e.g., Förster et al. 2005; Witzke and Giesler 2007; Thomas et al. 2009). Chemically, the pegmatites are enriched in Nb>Ta, Y, REE, Sc, Ti, Zr, Be, Th, U, Li, and F, which place them into the family

of niobium–yttrium–fluorine (NYF) pegmatites typically associated with metaluminous to weakly peraluminous, post-orogenic to anorogenic A-type granites (e.g., Černý 1991).

The uraninite (sample G101) is from the main, medium- to coarse-grained, weakly seriate textural variant of the granite. It was collected from an abandoned quarry on the eastern slope at the elevation "Schoorstein", SE of Thiemendorf (see Fig. 2b). Typical for evolved STZ granites, sample G101 displays low to moderate albitization of feldspars, sericitization of plagioclase, and muscovitization/chloritization of siderophyllite. However, its chemical composition demonstrates predominantly closed-system behavior, significantly different from that characterizing the Si-depleted and Al-enriched "episyenites" known from the Königshain pluton (cf. Hecht et al. 1999). Sample G101, which has the following major-element composition (in wt%): $SiO_2$ – 76.2, $TiO_2$ – 0.07, $Al_2O_3$ – 12.8, $Fe_2O_3$(tot) – 0.99, MnO – 0.03, MgO – 0.06, CaO – 0.61, $Na_2O$ – 3.70, $K_2O$ = 4.61, $P_2O_5$ = 0.013, $H_2O^+$ - 0.61, $CO_2$ – 0.13, total – 99.8, A/CNK = 1.05, corresponds to "unaltered" Königshain granite *sensu* Hecht et al. (1999). Trace-element data are reported in the Supplementary electronic material.

Locally, molybdenite crystals are well formed and suggest growth in open space within fractured granite mush (Fig. 3). The molybdenite sample in this study is from the main (equigranular) granite facies, exposed in quarry 1 (formerly quarry Jenichen), SE of the cliff Hochstein near Königshain (Fig. 2b).

## Analytical techniques

### Electron Microprobe

Uraninite and the other radioactive accessory minerals were analyzed using a JEOL thermal field-emission electron-microprobe JXA-8500 F (HYPERPROBE) at Deutsches GeoForschungsZentrum (GFZ) in Potsdam.

During routine full-element analysis of accessory minerals, beam conditions involved an accelerating voltage of 15 kV, a beam current of 40 nA, and different beam diameters depending on the size of the grains (focused beam or 1–2 μm beam diameter). The counting times on the peaks were 20 s for Ca, Fe, Al, P and Si, 30 s for Y, 50 s for the REEs, and 100 s for Pb, Th and U. The matrix corrections were performed according to the Armstrong-CITZAF method (Armstrong 1995).

A different analytical setup was used for the dating of uraninite. For this purpose, only its four most abundant elements U (Mβ, PET), Th (Mα, PET), Pb (Mα and Mβ, PET and PETH),

and Y (Lα, TAP) were analyzed. Measurements were performed during three analytical sessions and involved different accelerating voltages and beam currents (15 kV and 20 kV, 20 nA and 40 nA). The counting times on the peaks were 50–100 s for the elements and, in each case, half time for background counts on both sides of the peak. The small overlapping corrections of Th Mγ with U Mβ, Y Lβ with Pb Mα, and U Mζ with Pb Mβ were done offline. See Supplementary electronic material for analytical details, detection limits, and typical analytical uncertainties.

Repeated measurements of the same spot during different sessions yielded corresponding results within a mean error of ~15 m.y. Complementary measurements, which were made for some selected spots using a CAMECA SX100, were in full accord with those conducted with the JEOL maschine (see Supplementary electronic material).

Mass Spectrometry (Re–Os)

Molybdenite was separated as a drilled powder from a fresh quarry sample. Care was taken to sample several small crystals in their entirety to overcome any possibility of parent-daughter ($^{187}$Re–$^{187}$Os) decoupling (Stein et al. 2001, 2003). Further, a large separate of 135 mg was analyzed with the anticipation of low Re and a geologically young age (Variscan). Rhenium and Os concentrations were determined by isotope dilution. Inverse *aqua regia* in a thick-walled Carius tube was used to dissolve and equilibrate the sample with a well-calibrated mixed-double Os spike ($^{185}$Re–$^{188}$Os–$^{190}$Os). The sample was digested at 250 $^{o}$C for 12 hours. Osmium was distilled as $OsO_4$ from the *aqua regia* and captured in cold HBr. Osmium was further purified by micro-distillation. Rhenium was recovered by anion exchange chromatography following further dilution of *aqua regia* to reduce the Mo concentration to below 3 mg/mL. Rhenium was further cleaned using a single anion exchange bead and a series of solutions mimicking the column chromatography procedure.

Both elements were loaded on individual Pt filaments with $Ba(NO_3)_2$ and Ba(OH) activators for Re and Os, respectively. Rhenium and Os isotopic ratios were measured by negative thermal ion mass spectrometry (NTIMS), first on a single-collector NBS 12-inch, 90-degree mass spectrometer, and then on a multi-collector Triton mass spectrometer using splits from aliquots of the same purified Re and Os. Raw ratios on both instruments are corrected for oxygen-isotope composition. The Königshain sample was among many run on both mass

spectrometers at AIRIE to establish a base of comparative data between molybdenites run on an older single-collector and a new multi-collector machine.

The Re–Os age was calculated using the age equation $(^{187}Os)_m = (^{187}Os)_i + {}^{187}Re\ (e^{\lambda t} - 1)$ with the error propagation incorporating spike calibration, blank concentrations for Re and Os, blank Os-isotopic composition, measured ratios, and the $^{187}Re$ decay constant error. Ages calculated from data derived from each machine are identical within analytical precision. The AIRIE labs routinely run the Henderson molybdenite as their reference material (Markey et al. 2007); this Henderson Reference Material® 8599 and accompanying Report of Investigation is available from the US National Institute of Standards and Technology (NIST). An additional test for the accuracy of the Re–Os molybdenite ages is provided by the comparison of U–Pb zircon ages and Re–Os molybdenite ages obtained from the same rock or mineral deposits. For instance, independent dating of Bulgarian Cu–Au mineralization by the U–Pb zircon and Re–Os molybdenite methods gave identical ages (cf. von Quadt et al. 2002, 2005, Zimmerman et al. 2008).

## Results

*Composition and U–Th–total Pb ages of uraninite*

From the magmatic Th–U-bearing accessory minerals present in the granite sample (zircon, monazite-(Ce), xenotime-(Y), uraninite, thorite-xenotime solid solutions), we selected uraninite for chemical dating. The uraninite grains contain simultaneously large concentrations of U, Th, and Pb, are hosted in unaltered siderophyllite, and lack signs of alteration (see below). Xenotime-(Y) and common monazite-(Ce) (Fig. 4a, b) have too low Th plus U (and correspondingly Pb) contents to be analytically suitable for microprobe dating. Moreover, some of these monazite-(Ce) grains experienced alteration, resulting in mobilization of Th and formation of tiny grains of secondary thorite (cf. Fig. 4b). A few grains of Th-rich (>20 wt% $ThO_2$) monazite-(Ce) readily decomposed under the electron beam, possibly reflecting metamictization. Metamict thorite–xenotime solid solutions rich in Fe, Nb, and U (Fig. 4c, d) were also destabilized under the electron beam. Unaltered zircon has incorporated concentrations of Th and U at a level too low as that sufficiently large concentrations of radiogenic Pb were produced that would permit microprobe dating with fair error (cf. Thomas et al. 2009).

Two, euhedral-subhedral grains of uraninite, 50 μm and 15 μm across (Fig. 5), were analyzed and dated by electron microprobe. Although these grains are zoned (cf. Fig. 5b, d), the overall compositional variability is small (Table 1). Uraninite is moderately rich in Th ($4.5<ThO_2<7.4$ wt%) and Y ($1.9<Y_2O_3<4.7$ wt%) and contains several oxide wt% of REE ($3.7<REE_2O_3<8.7$ wt%). Concentrations of alteration-fingerprinting non-stoichiometric elements, such as P, Si, Al, Ca, or Fe, are below their respective detection limits.

For dating, a total of 60 single-spot analyses of Th, U, Pb, and Y were obtained on both uraninite grains, evenly distributed over the grains and encompassing all chemical zones larger than 5 μm (the excitation volume of the electron beam). The apparent single-point ages, which range from 316 to 339 Ma (Table 2), do not correlate with the zonation patterns reflecting variations in U–Th–(Y+REE) space (cf. Fig. 5). Redistribution of Pb and the formation of secondary galena in uraninite and at the rims of uraninite is known from hydrothermally altered uraninite of early Proterozoic and older age (e.g., Janeczek 1999). Such secondary redistribution would reduce the chemical age of the uraninite. However, mapping of the dated uraninite grains did not show any evidence for Pb mobilization. Furthermore, even spots close to cracks or near rims of the grains yield ages that overlap within error with those obtained in the cores or in domains away from cracks. The average error for each analysis is 15 m.y., as derived from repeated measurements of the same spot and the counting statistics. Considering a constant error of ± 15 m.y. for each of the 60 spot analyses results in a weighted mean Th–U–total Pb age of 328.6 ± 1.9 Ma ($2\sigma$; MSWD = 1.0; Fig. 6), using the ISOPLOT/EX program of Ludwig (1999). The use of a larger constant error of ± 20 m.y. would only slightly increase the error of the weighted mean Th–U–total Pb age to ± 2.5 Ma, but would not affect the calculated age.

*Re-Os on molybdenite*

The Re-Os isotopic data and analytical details are presented in Table 3. Rhenium and Os were chemically isolated from a single molybdenite mineral separate. An aliquot of both Re and Os was run on the single-collector (NBS) and multi-collector (Triton) mass spectrometers with excellent agreement. Rhenium concentrations are moderately low (3.5 ppm), as is commonly the case for granites associated with Mo–W–Sn mineralization (Stein 2006; Raith and Stein 2006). The radiogenic $^{187}Os$ (11.9 ppb) is far out of reach of any blank issues. Common Os was determined, and is insignificant. The data are blank corrected, but as is nearly always the

case, blank is irrelevant for Re–Os dating of molybdenite. The Re and Os blanks are well under 1 pg, with a blank $^{187}Os/^{188}Os$ ratio of 0.257 (see Table 3 footnotes).

We report two Re-Os ages for this molybdenite sample, one derived from a multi-collector (Triton) at 327.0 ± 1.3 Ma and a second derived from a single-collector mass spectrometer (NBS) at 327.6 ± 1.1 Ma (Table 3). If we consider only analytical uncertainty (removing the $^{187}Re$ decay constant uncertainty), the ages still overlap at 2σ (Table 3, 327.0 ± 0.7 and 327.6 ± 0.4 Ma). Note, however, for comparison of age uncertainties derived from different isotopic systems, the full uncertainty with the decay constant error must be reported.

Re–Os ages were calculated assuming an initial $^{187}Os/^{188}Os$ ratio of 0.2 and the $^{187}Re$ decay constant of Smoliar et al (1996). The extremely high $^{187}Re/^{188}Os$ ratios in nearly all molybdenites preclude any change in the age using higher assumed initial $^{187}Os/^{188}Os$ ratios.

**Discussion**

The Th–U–total Pb age of uraninite (328.6 ± 1.9 Ma) and the Re–Os age of molybdenite (327.0 ± 1.3 Ma and 327.6 ± 1.1) are indistinguishable and overlap at the 2σ confidence level. Both ages date the Königshain granite at 10–15 Ma older than previous estimates (Hammer et al. 1999; Thomas et al. 2009). There are several possible reasons for the discrepancy in our age results compared to previous work. As typical for evolved granites from the STZ (e.g., Irber et al. 1997, Förster et al. 1999, Breiter et al. 2006), zircon from the Königshain granite may have suffered from alteration, giving rise to a disturbed isotopic system. The 315 ± 6 Ma zircon age of Hammer et al. (1999) was obtained by the $^{207}Pb/^{206}Pb$ evaporation method. An inherent assumption of this method is that the individual zircon grains are concordant – an assumption that cannot be tested from the analytical data. Lead loss from metamict zircon may occur continuously or episodically in time and results in $^{207}Pb/^{206}Pb$ ages that are too young. Minor Pb loss will not be readily apparent in the $^{207}Pb/^{206}Pb$ ratio of Phanerozoic zircon analyzed by the evaporation method, but will shift the $^{207}Pb/^{206}Pb$ age to a too young age (Romer 2003). The paper of Thomas et al. (2009) reports only the age datum, but lacks information on the uncertainty of the 320 Ma age and a listing of the individual spot analyses used for age calculation from monazite, xenotime, and uraninite. Thus, it is impossible to judge the reliability of this age estimate. Altogether, our new age data suggest that Variscan magmatism in the Lausitz Block started about 10 Ma earlier than all previous estimates imply.

Relative to adjacent regions of the Saxo-Thuringian Zone (cf. Figs. 2 and 7), the Königshain granite formed during the same magmatic period that gave rise to the gabbroic to granitic magmatism in the *Elbe Zone* (Meissen Massif) to the immediate west (~335–325 Ma; Wenzel et al. 1997; Kurze et al. 1998; Nasdala et al. 1999; Hofmann et al. 2009) and the monzodioritic to granitic rocks forming the northeastern section of the *Mid-German Crystalline Zone* (~335–325 Ma; Anthes and Reischmann 2001; Zeh and Will 2010). It is a few Ma younger than the nearby granitic rocks from the Saxon Granulite Massif (335–333 Ma; von Quadt 1993; Kröner et al. 1998; Nasdala et al. 1998). The Königshain granite was emplaced at about the same time as the most voluminous granite magmatism in the Erzgebirge–Vogtland Zone, which started sometime between 328 and 325 Ma and commenced until about 318 Ma (e.g., Förster et al. 1999, 2009; Romer et al. 2007; Förster and Romer 2010; Tichomirowa and Leonhardt 2010).

The geochronology of late-Variscan magmatism in the LB, however, is not yet fully understood. One unresolved problem is whether the magmatic processes were continuous or episodic as in most, if not all sub-regions of the Saxo-Thuringian Zone. In particular, additional age data are warranted for the amphibole-bearing granites, where single-zircon evaporation ages are fraught by large errors of 10 m.y..

According to our data, the Königshain granite in the Lausitz does not have a unique position within the overall timeframe of igneous activities in this segment of the STZ and the Bohemian Massif, but was generated during the same episode as the bulk of rocks in the westerly neighbouring block. The distribution of late-Variscan magmatism is controlled spatially and temporally by the large-scale evolution of the Variscan Orogen. In the Bohemian Massif, the close spatial relation between high-grade metamorphic rocks (peak metamorphism at c. 340 Ma) and the voluminously most important granites (c. 327–318 Ma) is notable (cf. Finger et al. 2009, Förster and Romer 2010, Kroner and Romer 2010). The dominant structural elements are NW–SE striking dextral shear zones (e.g., Inner Lausitz Fault, Elbe Fault Zone, Gera–Jachymov Fault Zone, Franconian Line; Fig. 7) that were active during the exhumation of the Variscan metamorphic complexes (c. 340 to 330 Ma) and along which rocks of contrasting Variscan metamorphism are exposed. These zones were repeatedly reactivated. In the STZ, the metamorphic nappes of the Allochthonous Domain were transported from beneath the Bohemian Massif to the northwest; to the south of the Tepla–Barandian Unit, in the Moldanubian Zone, corresponding nappes were thrust to the southeast. The final emplacement of these nappes with thrusting over molasses-type

sediments and folding of these foreland sediments of the Thrust–and–Wrench Zone (Hahn et al. 2010; Kroner and Goerz 2010), which is related to the collision of the Cadomian blocks of the Protoalps (Vollbrecht et al. 1989), is probably contemporaneous with the emplacement of the 327–318 Ma-old granites.

The geochemical variability of the Variscan granites of the Saxo-Thuringian Zone reflects the contrasting involvement of volcanic and sedimentary rocks in the granite source (Förster and Romer 2010). These source rocks had been deposited on the Gondwana shelf and were subducted during the Variscan orogeny. The metamorphic equivalents of these rocks form an intergral part of the nappes of the Variscan metamorphic complexes, such as the Erzgebirge (Rötzler and Plessen 2010). The rapid exhumation of these metamorphic units transported also heat into the middle and upper crust, which eventually resulted in local melting, whereas the late reactivation of the NW–SE striking lineaments in conjunction with the collision to the Protoalps, reactivated the structural elements that controlled granite emplacement

The Lausitz Block was not subducted during the Variscan orogeny and experienced only minor Variscan metamorphism and deformation. It consists predominantly of crust that was largely consolidated during the Cadomian orogeny (e.g., Linnemann et al., 2004, 2010). Possibly, this lack of Variscan overprint and, in particular, the complete absence of high-grade metamorphic nappes account for the scarcity of Variscan granite magmatism in the Lausitz in relation to the neighboring Erzgebirge. The Königshain granite in the eastern Lausitz is close to the large, deep-seated *Inner Lausitz fault*, which is part of a late Variscan shear zone forming the NE border of this tectonic block. The biotite granite of Stolpen is crossed by the *Stolpen–Klotzsche Fault*. Granite magmatism in the Erzgebirge–Vogtland Zone and the Lausitz Block apparently was synchronous. Thus, emplacement of Variscan granites in the LB may be controlled by the same processes as for the Saxo-Thuringian and the Moldanubian zones, i.e., the reactivation of older strike-slip zones during the collision of the Protoalps with the Bohemian Massif.

## Acknowledgements

Aaron Zimmerman (AIRIE Program) is thanked for his Re–Os analytical efforts. The Re–Os work was supported by a Helmholtz-Humboldt research award to HJS. All specimens were kindly provided by Wolfram Lange (Zittau), who also helped with the compilation for Figure 2. Martin Ziemann (Potsdam) supported HF and DR in running the ISOPLOT/EX program for

uraninite dating. Editorial comments by W.-C. Dullo and suggestions by four reviewers supported in improving the paper.

## References

Anthes G, Reischmann T (2001) Timing of granitoid magmatism in the eastern mid-German crystalline rise. J Geodyn 31:119–143

Armstrong JT (1995) CITZAF: a package of correction programs for the quantitative electron microbeam X-ray-analysis of thick polished materials, thin films, and particles, Microbeam Anal 4:177–200

Breiter K (2008) Mineral and textural evolution of subvolcanic A-type granite: Hora Svaté Kateřiny stock, Krušné Hory Mts., Czech Republic. Z geol Wiss **36**:365–382

Breiter K, Förster H-J, Škoda R (2006) Extreme P-, Bi-, Nb-, Sc-, U-, and F-rich zircon from fractionated perphosphorus granites: the peraluminous Podlesí granite system, Czech Republic. Lithos 88:15–34.

Černý P (1991) Rare-element granitic pegmatites. I. Anatomy and internal evolution of pegmatite deposits. Geosci Canada 18:46–67

Eidam J, Götze J (1991) The granitic massif of Königshain–Arnsdorf (Lusatian Anticlinal Zone): an example of a reversely zoned pluton. Chem Erde 51:55–71

Finger F, Gerdes A, René M, Riegler G (2009) The Saxo-Danubian Granite Belt: magmatic response to postcollisional delamination of mantle lithosphere below the southwestern sector of the Bohemian Massif (Variscan orogen). Geol Carpathica 60:205–212

Förster H-J (1999) The chemical composition of uraninite in Variscan granites of the Erzgebirge, Germany. Miner Mag 63:239–252

Förster H-J (2006) Composition and origin of intermediate members of the system thorite–xenotime–zircon–coffinite. Lithos 88:35–55

Förster H-J, Rhede D (2005) The Be–Ta-rich granite of Seiffen (eastern Erzgebirge, Germany): accessory-mineral chemistry, composition, and age of a post-collisional Li–F granite of A-type affinity. N Jb Mineral Abh 183: 307–321.

Förster H-J, Romer RL (2010) Carboniferous Magmatism. In: Linnemann U, Romer RL (eds) Pre-Mesozoic Geology of Saxo-Thuringia – From the Cadomian Active Margin to the Variscan Orogen. Schweizerbart, Stuttgart, 287–308

Förster H-J, Tischendorf G, Trumbull RB, Gottesmann B (1999): Late-collisional granites in the Variscan Erzgebirge (Germany). J Petrol 40:1613–1645.

Förster H-J, Tischendorf G, Rhede D, Naumann R, Gottesmann B, Lange W (2005) Cs-rich lithium micas and Mn-rich lithian siderophyllite in miarolitic NYF pegmatites of the Königshain granite, Lausitz, Germany. N Jb Mineral Abh 182:81–93.

Förster H-J, Rhede D, Hecht L (2008) Chemical composition of radioactive accessory minerals: implications to the evolution, alteration, age, and uranium fertility of the Fichtelgebirge granites (NE Bavaria, Germany). N Jb Mineral Abh 185:161–182.

Förster H-J, Romer RL, Gottesmann B, Tischendorf G, Rhede D (2009) Are the granites of the Aue–Schwarzenberg Zone (Erzgebirge, Germany) a major source for metalliferous ore deposits? a geochemical, Sr–Nd–Pb isotopic, and geochronological study. N Jb Mineral Abh 186:163–184

Hahn et al (2010) Early Carboniferous synorogenic sedimentation in the Saxo-Thuringian Basin and the adjacent Allochthonous Domain. In: Linnemann U, Romer RL (eds) Pre-Mesozoic Geology of Saxo-Thuringia – From the Cadomian Active Margin to the Variscan Orogen. Schweizerbart, Stuttgart, 171–192

Hammer J (1996) Geochemie und Petrogenese der cadomischen und spätvariszischen Granitoide der Lausitz. Freib Forschungsh C463: 107 pp.

Hammer J, Eidam J, Röber B, Ehling C (1999) Prävariszischer und variszischer granitoider Magmatismus am NE-Rand des Böhmischen Massivs – Geochemie und Petrogenese. Z geol Wiss 27:401–415.

Harlov D.E., Wirth R., Hetherington C.J. (2007) The relative stability of monazite and huttonite at 300–900 $^{o}$C and 200–1000 MPa: Metasomatism and the propagation of metastable mineral phases. Amer Mineral **92**:1652–1664

Hecht L, Thuro K, Plinninger R, Cuney M (1999) Mineralogical and geochemical characteristics of hydrothermal alteration and episyenitization in the Königshain granites, northern Bohemian Massif, Germany. Int J Earth Sci 88:236–252.

Hetherington, CJ, Harlov DE (2008) Metasomatic thorite and uraninite inclusions in xenotime and monazite from granitic pegmatites, Hidra anorthosite massif, southwestern Norway: Mechanics and fluid chemistry. Amer Mineral 93:806-820.

Hofmann M, Linnemann U, Gerdes A, Ullrich B, Schauer M (2009) Timing of dextral strike-slip processes and basement exhumation in the Elbe Zone (Saxo-Thuringian Zone): the final pulse of the Variscan Orogeny in the Bohemian Massif constrained by LA-SF-ICP-MS U–Pb zircon data. In: Murphy JB, Keppie JD, Hynes A (Eds) Ancient and Modern Orogens. Geol. Soc. London, Spec Publ 327:197–214

Irber W, Förster H-J, Hecht L, Möller P, Morteani G (1997) Experimental, geochemical, mineralogical, and O-isotope constraints on the late-magmatic history of the Fichtelgebirge granites (Germany). Geol Rundsch 86:Suppl.,S110–S124.

Janeczek J (1999) Mineralogy and geochemistry of natural fission reactors in Gabon. Rev Mineral 38:321–392

Kempe U (2003) Precise electron microprobe age determination in unaltered uraninite: consequences on the intrusion age and the metallogenetic significance of the Kirchberg granite (Erzgebirge, Germany). Contrib Mineral Petrol 145:107–118

Kováříková P, Siebel W, Jelínek E, Štemprok M, Kachlík V, Holub FV, Blecha V (2010) Dioritic intrusions of the Slavkovský les (Kaiserwald), Western Bohemia: their origin and significance in late Variscan granitoid magmatism. Int J Earth Sci 99:545–565.

Kröner A, Hegner E, Hammer J, Haase G, Bielicki K-H, Krauss M, Eidam J (1994) Geochronology and Nd–Sr systematics of Lusatian granites: significance for the evolution of the Variscan orogen in east-central Europe. Geol Rundsch 83:357–376

Kröner A, Jaeckel P, Reischmann T, Kroner U (1998) Further evidence for an early Carboniferous (340 Ma) age of high-grade metamorphism in the Saxonian granulite complex. Geol Rundsch 86:751–766

Kroner U, Görz I (2010) Variscan assembling of the Allochthonous Domain of the Saxo-Thuringian Zone – a tectonic model. In: Linnemann U, Romer RL (eds) Pre-Mesozoic Geology of Saxo-Thuringia – From the Cadomian Active Margin to the Variscan Orogen. Schweizerbart, Stuttgart, 271–286

Kroner U, Romer RL (2010) The Saxo-Thuringian Zone – tip of the Armorican spur and part of the Gondwana plate. In: Linnemann U, Romer RL (eds) Pre-Mesozoic Geology of Saxo-Thuringia – From the Cadomian Active Margin to the Variscan Orogen. Schweizerbart, Stuttgart, 371–394

Kroner U, Hahn T, Romer RL, Linnemann U (2007) The Variscan orogeny in the Saxo-Thuringian – heterogeneous overprint of Cadomian/Palaeozoic peri-Gondwana crust. In: Linnemann U, Nance RD, Kraft P, Zulauf G (Eds) The Evolution of the Rheic Ocean: from Avalonian–Cadomian Active Margin to Alleghenian–Variscan Collision. Geol Soc Amer, Spec Pap 423:153–172

Kroner U, Romer RL, Linnemann U (2010) The Saxo-Thuringian Zone of the Variscan Orogen as part of Pangea. In: Linnemann U, Romer RL (eds) Pre-Mesozoic Geology of Saxo-Thuringia – From the Cadomian Active Margin to the Variscan Orogen. Schweizerbart, Stuttgart, 3–16

Kurze M, Seifert Th, Weber H, Henjes-Kunz F (1998) Petrographie, Geochemie und Altersstellung der Lamprophyr-Gänge des Elbtalschiefergebirges (Sachsen). Z geol Wiss 26:193–202

Linnemann U, McNaughton NJ, Romer RL, Gehmlich M, Drost K, Tonk C (2004) West African Provenance for Saxo-Thuringia (Bohemian Massif): Did Armorica ever leave pre-Pangean Gondwana? – U/Pb-SHRIMP zircon evidence and the Nd-isotopic record. Int J Earth Sci 93:683–705

Linnemann U, Romer RL, Gerdes A, Jeffries TE, Drost K, Ulrich J (2010) The Cadomian Orogeny in the Saxo-Thuringian Zone. In: Linnemann U, Romer RL (eds) Pre-Mesozoic Geology of Saxo-Thuringia – From the Cadomian Active Margin to the Variscan Orogen. Schweizerbart, Stuttgart, pp. 37–58

Ludwig KR (1999) Users manual for ISOPLOT/EX, version 2. A geochronological toolkit for Microsoft Exel. Berkeley Geochronological Center, Spec Publ 1a, 43p.

Markey RJ, Hannah JL, Morgan JW, Stein, HJ (2003) A double spike for osmium analysis of highly radiogenic samples. Chem Geol 200:395-406

Markey R, Stein HJ, Hannah, JL, Zimmerman A, Selby D, Creaser RA (2007) Standardizing Re-Os geochronology: a new molybdenite Reference Material (Henderson, USA) and the stoichiometry of Os salts. Chem Geol 244:74–87

Möbus G, Lindert W (1967) Das Granitmassiv von Königshain bei Görlitz (Oberlausitz). Abh Dtsch Akad Wissenschaft Kl Bergbau Hüttenwesen Montangeol 1:81–160

Nasdala L, Pidgeon RT, Wolf D, Irmer G (1998) Metamictization and U–Pb isotopic discordance in single zircons: a combined Raman microprobe and SHRIMP ion probe study. Mineral Petrol 62:1–27

Nasdala L, Wenzel Th, Pidgeon RT, Kronz A (1999) Internal structures and dating of complex zircons from the monzonite from Leuben/Saxony. Chem Geol 156:331–341

Raith JG, Stein HJ (2006) Variscan ore formation and metamorphism at the Felbertal scheelite deposit (Austria): constraining tungsten mineralisation from Re–Os dating of molybdenite: Contrib Mineral Petrol 152:505–521

Romer RL (2003) Alpha-recoil in U–Pb geochronology: effective sample size matters. Contrib Mineral Petrol145:481–491

Romer RL, Thomas R, Stein HJ, Rhede D (2007) Dating multiply overprinted Sn-mineralized granites – examples from the Erzgebirge, Germany. Mineral Depos 42:337–359

Romer RL, Förster HJ, Štemprok M (2010) Age of late-Variscan magmatism in the Altenberg–Teplice Caldera (Eastern Erzgebirge/Krušné hory). N Jb Mineral Abh 187:289–305

Rötzler J, Romer RL (2010) The Saxon Granulite Massif: a key area for the geodynamic evolution of Variscan central Europe. In: Linnemann U, Romer RL (eds) Pre-Mesozoic Geology of Saxo-Thuringia – From the Cadomian Active Margin to the Variscan Orogen. Schweizerbart, Stuttgart, 233–252

Rötzler K, Plessen B (2010) The Erzgebirge: a pile of ultrahigh- to low-pressure nappes of early Palaeozoic rocks and their Cadomian basement. In: Linnemann U, Romer RL (eds) Pre-Mesozoic Geology of Saxo-Thuringia – From the Cadomian Active Margin to the Variscan Orogen. Schweizerbart, Stuttgart, 253–270

Siebel W, Chen F, Satir M (2003) Late-Variscan magmatism revisited: new implications from Pb-evaporation zircon ages on the emplacement of redwitzites and granites in NE Bavaria. Int J Earth Sci 92:36–53

Siebel W, Shang CK, Presser V (2010): Permo-Carboniferous magmatism in the Fichtelgebirge: dating the final intrusive pulse by U-Pb, $^{207}Pb/^{206}Pb$ and $^{40}Ar/^{39}Ar$ geochronology. Z geol Wiss **38**:85–98

Smoliar MI, Walker RJ, Morgan JW (1996) Re–Os ages of group IIA, IIIA, IVA and IVB iron meteorites. Science 271:1099–1102

Stein HJ (2006) Low-rhenium molybdenite by metamorphism in northern Sweden: recognition, genesis, and global implications. Lithos 87:300–327

Stein H, Scherstén A, Hannah J, Markey R (2003) Sub-grain scale decoupling of Re and $^{187}Os$ and assessment of laser ablation ICP-MS spot dating in molybdenite. Geochim Cosmochim Acta 67:3673–3686

Stein HJ, Markey RJ, Morgan JW, Hannah JL, Scherstén A. (2001) The remarkable Re–Os chronometer in molybdenite: how and why it works. Terra Nova 13:479–486

Thomas R, Davidson P, Rhede D, Leh M (2009) The miarolitic pegmatites from the Königshain: a contribution to understanding the genesis of pegmatites. Contrib Mineral Petrol 157:505–523

Tichomirowa M, Leonhardt D (2010) New age determinations (Pb/Pb zircon evaporation, Rb/Sr) on the granites from Aue–Schwarzenberg and Eibenstock, Western Erzgebirge, Germany. Z geol Wiss 38:99–123

Tischendorf G, Pälchen W, Röllig G, Lange H (1987) Formationelle Gliederung, petrographisch-geochemische Charakteristik und Genese der Granitoide der Deutschen Demokratischen Republik. Chem Erde 46:7–23

Ulrych J, Pešek J, Štěpánková-Svobodova J, Bosák P, Lloyd FE, von Seckendorf V, Lang M, Novák JK (2006) Permo-Carboniferous volcanism in late Variscan continental basins of the Bohemian Massif (Czech Republic): geochemical characteristics. Chem Erde 66:37–56

Vollbrecht A, Weber K, Schmoll J (1989) Structural model for the Saxothuringian-Moldanubian suture in the Variscan basement of the Oberpfalz (Northeastern Bavaria, F.R.G.) interpreted from geophysical data. Tectonophysics 157:123–133

von Quadt A (1993) The Saxonian granulite massif; new aspects from geochronological studies. Geol Rundsch 82:516–530

von Quadt A, Peytcheva I, Kamenov B, Fanger L, Heinrich CA, Frank M (2002) The Elatsite porphyry copper deposit in the Panagyurishte ore district, Srednogorie zone, Bulgaria: U–Pb zircon geochronology and isotope-geochemical investigations of magmatism and ore genesis. In: Blundell DJ, Neubauer F, von Quadt A (eds) The Timing and Location of Major Ore Deposits in an Evolving Orogen. Geol Soc Spec Publ 204:119–135

von Quadt A, Moritz R, Peytcheva I, Heinrich C (2005) Geochronology and geodynamics of Upper Cretaceous magmatism and Cu–Au mineralization in the Panagyurishte region of the Apuseni–Banat–Timok–Srednogorie belt (Bulgaria). Ore Geol Rev 27:95–126

Wenzel Th, Mertz DF, Oberhänsli R, Becker T, Renne PR (1997) Age, geodynamic setting, and mantle enrichment processes of a K-rich intrusion from the Meissen massif (northern Bohemian massif) and implications for related occurrences from the mid-European Hercynian. Geol Rundsch 86:556–570

Witzke T, Giesler T (2007) Wismut-Mineralien aus dem Königshainer Granit, Lausitz. Mineralien-Welt 18:14–19

Zeh A, Will TM (2010) The Mid-German Crystalline Zone. In: Linnemann U, Romer RL (eds) Pre-Mesozoic Geology of Saxo-Thuringia – From the Cadomian Active Margin to the Variscan Orogen. Schweizerbart, Stuttgart, 195–220

Zimmerman A, Stein HJ, Hannah JL, Kozelj D, Bogdanov K, Berza T (2008) Tectonic configuration of the Apusini–Banat–Timok–Srednogorie belt, Balkans–South Carpathians, constrained by high precision Re–Os molybdenite ages. Mineral Deposita 43:1–21

Author's addresses:

Hans-Jürgen Förster (corresponding author), Dieter Rhede & Rolf L. Romer, Deutsches GeoForschungsZentrum-GFZ, Telegrafenberg, D-14473 Potsdam, Germany, forhj@gfz-potsdam.de
Holly J. Stein, AIRIE Program, Department of Geosciences, Colorado State University, Fort Collins, CO 80523-1482, USA and Geological Survey of Norway, Trondheim 7491, Norway
Gerhard Tischendorf, deceased 10 December 2007

## Figure captions

**Fig. 1** Simplified map showing the principal domains of the Saxo-Thuringian Zone (after Kroner et al., 2010).

**Fig. 2** (a) Geologic sketch map showing major Variscan plutonic bodies (light grey) in the Saxo-Thuringian Zone between the Vogtland in the west and the Lausitz Block in the east; MGCZ = Mid-German Crystalline Zone. Geographic boundaries are shown for D (Germany), CZ (Czech Republic), and PL (Poland); (b) General geology in the region of Königshain–Arnsdorf (modified from Förster et al. 2005). Locations for the uraninite (G101) and molybdenite ($MoS_2$) samples are indicated.

**Fig. 3** Photograph of molybdenite-bearing sample hosted in Königshain granite, showing the late-magmatic intergrowth of quartz and K-feldspar with coarse molybdenite. Molybdenite separate used for Re–Os analyses was derived from this sample. Centimeter scale bar shown.

**Fig. 4** Secondary electron (SE) and back-scattered electron (BSE) images of magmatic radioactive accessory minerals accompanying uraninite in sample G101. (a) BSE image of a vaguely zoned grain of monazite-(Ce). Microprobe analyses reveal moderate Th concentrations ranging from 6.8 wt% $ThO_2$ (darkest areas) to 11.5 wt% $ThO_2$ (lightest areas), at continuously low contents of U ($0.2<UO_2<0.5$ wt%); (b) BSE image of a large, patchy-zoned monazite-(Ce) grain. Relicts of the initial magmatic growth patterns (bright) are preserved in its core. Tiny bright spots in domains appearing dark in BSE image refer to inclusions of huttonite–monazite-(Ce) solid solutions, which originated in response to fluid-induced dissolution–reprecipitation processes that mobilized Th and Si from the structure of the host (cf. Harlov et al. 2007, Hetherington & Harlov 2008, Förster et al. 2008); (c) BSE image of an unidentified Th–Y silicophosphate mineral mantled by a compositionally homogeneous monazite-(Ce). The mineral is finely and, in general, systematically zoned and displays remarkable structural dislocations. Mineralogically, it may represent a hydrous (microprobe analyses totaling to ~90 wt%) thorite–xenotime solid solution (cf. Förster 2006) rich in Fe, Nb, and U. Large-beam (to minimize destruction by the electron beam) single-spot analyses conducted in homogeneous areas of another grain of this mineral revealed the following elemental concentrations (as wt% oxide): $22<Th<23$, $14<Y<16$, $6.9<U<7.7$,

5.8<Nb<6.7, 4.9<Fe<5.5; (d) SE image of an altered, solitary subhedral grain of the Th–Y mineral with a radiation-damage halo in the surrounding feldspar host.

**Fig. 5** SE and BSE images of the two dated uraninite grains from sample G101 hosted in the Königshain granite. (a) SE image of uraninite 1, showing a high intensity of fracturing; zrc = zircon, sid = siderophyllite, qtz = quartz; (b) BSE image of uraninite 1, showing systematic zonation; (c) SE image of uraninite 2 surrounded by an alteration halo in the siderophyllite host produced by radioactive damage; (d) BSE image of uraninite 2 shows an irregular, patchy zonation. Dark areas are relatively richer in REE; bright areas are richest in U.

**Fig. 6** U–Th–total Pb single-spot ages (n = 60, 30 from each uraninite grain, 2σ error bars shown), and the weighted mean age for Königshain uraninite using ISOPLOT/EX (Ludwig 1999).

**Fig. 7** Sketch map of the northern part of the Bohemian Massif showing the distribution of late-Variscan granites grouped according to age (simplified and supplemented after Finger et al. 2009). References: compilations in Finger et al. (2009) and Rötzler and Romer (2010) and special papers of Kröner et al. (1994), Förster & Rhede (2005), Breiter (2008), Förster et al. (2009), Tichomirowa and Leonhardt (2010), Kováříková et al. (2010), and Siebel et al. (2010).

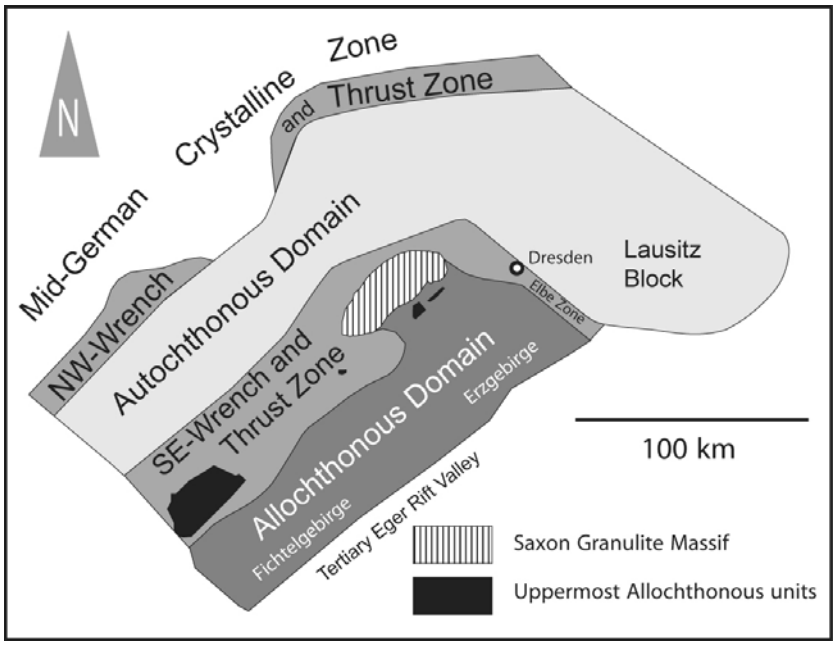


Figure 1

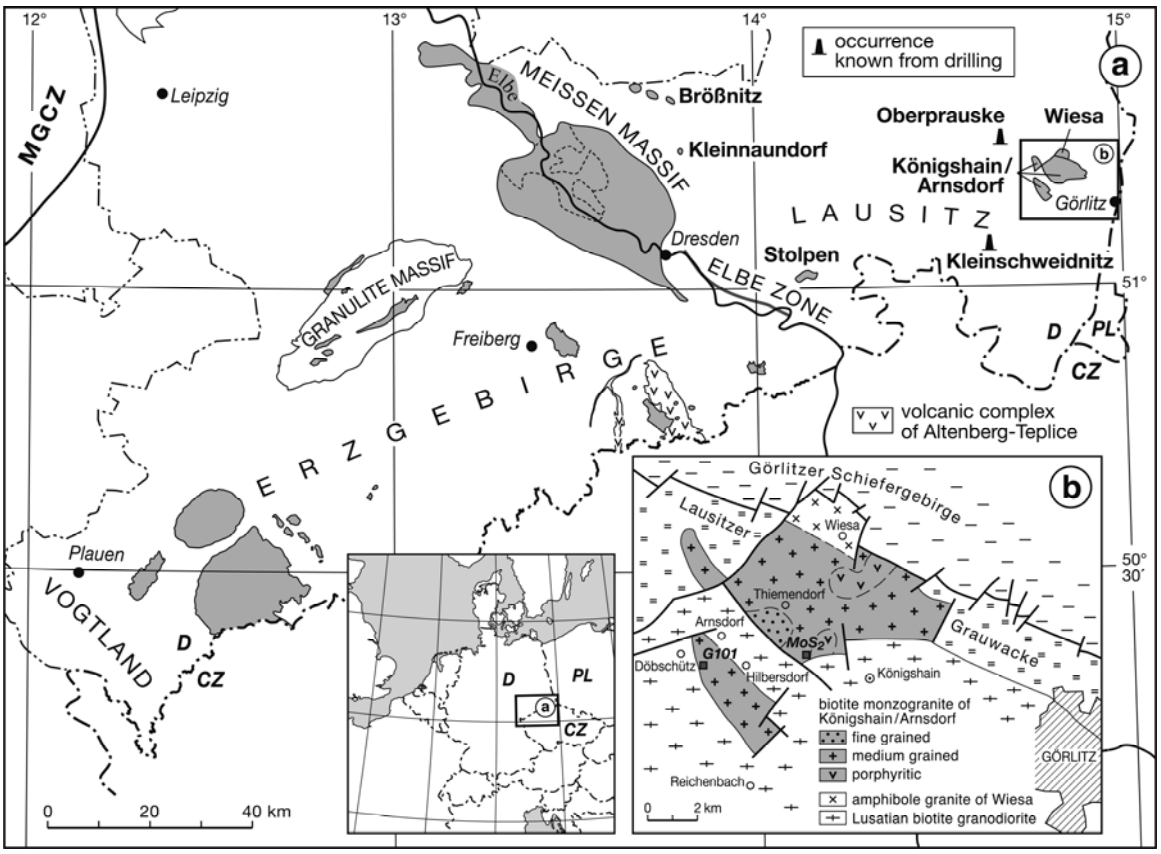


Figure 2

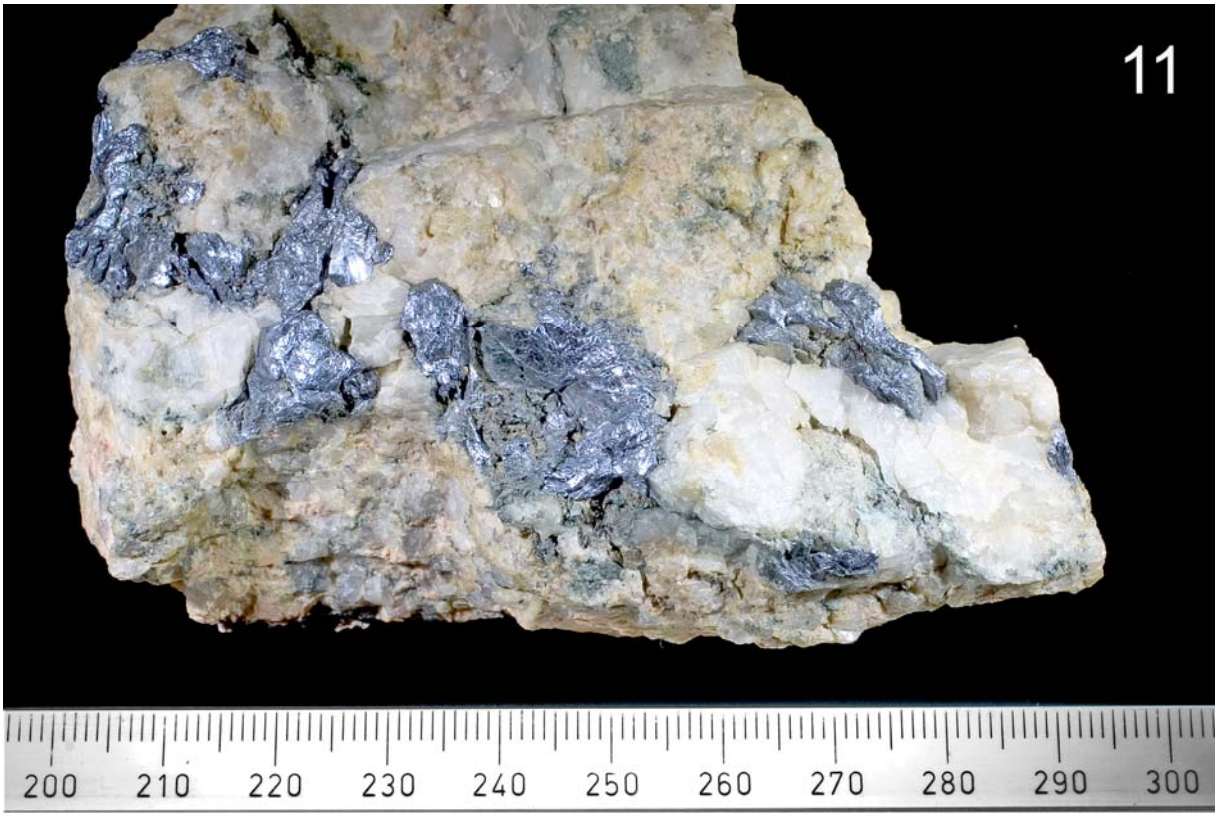


Figure 3

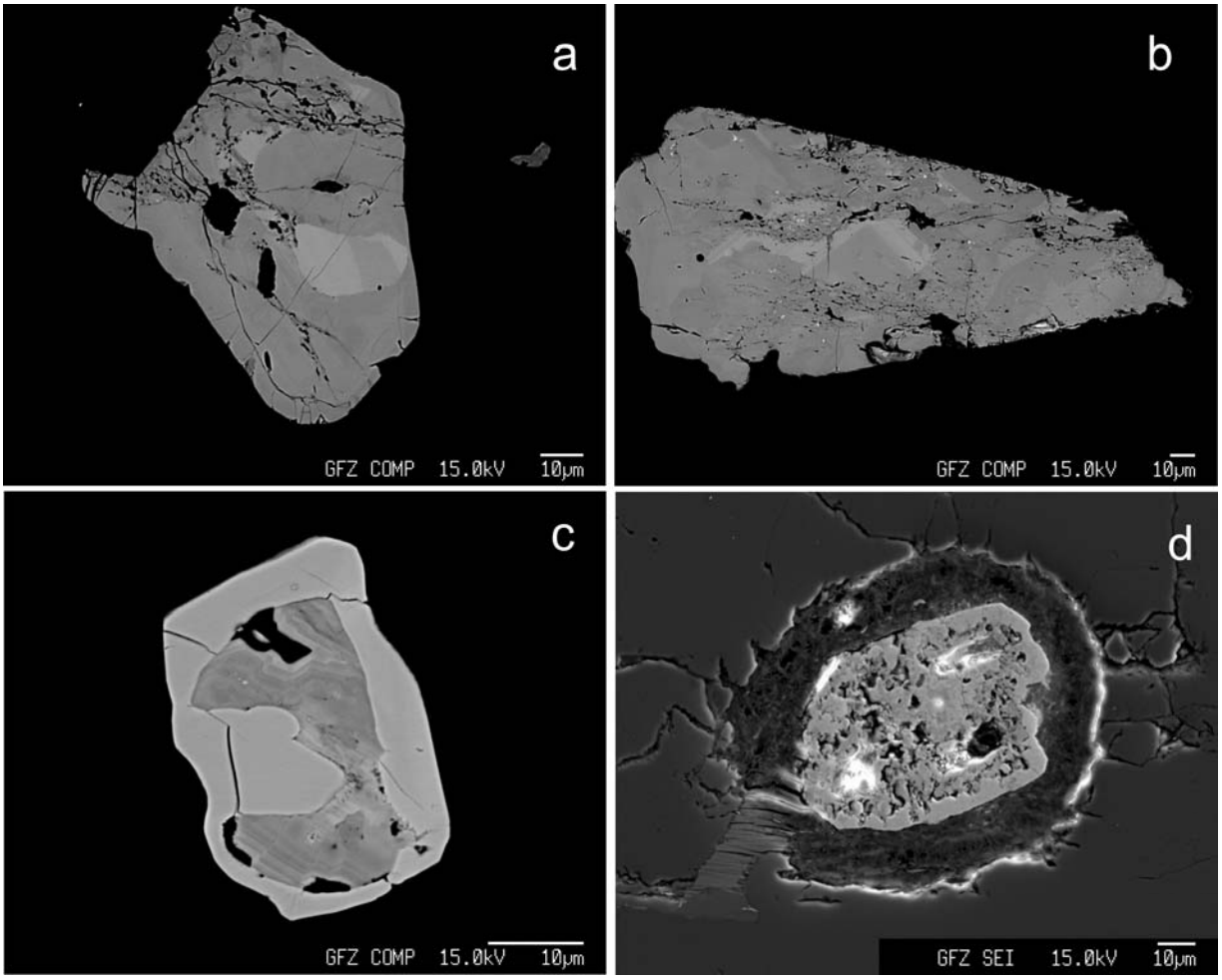
a
GFZ COMP 15.0kV 10µm
b
GFZ COMP 15.0kV 10µm
c
GFZ COMP 15.0kV 10µm
d
GFZ SEI 15.0kV 10µm

Figure 4

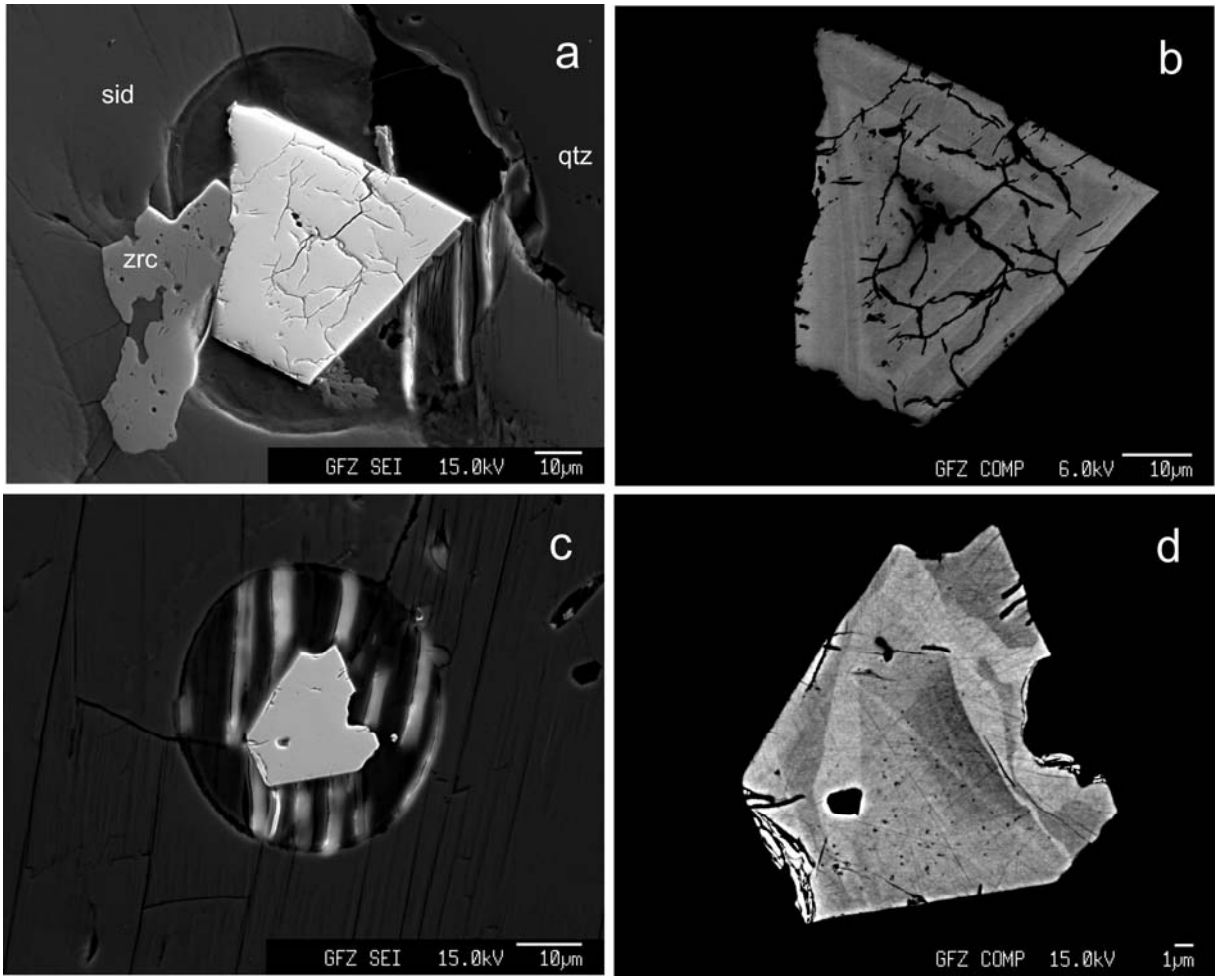


Figure 5

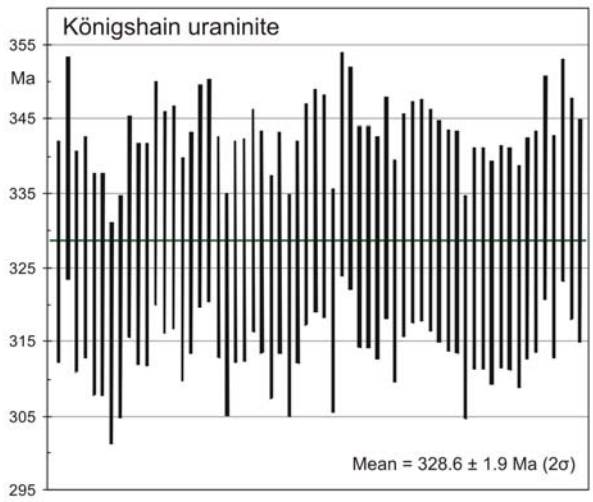


Figure 6

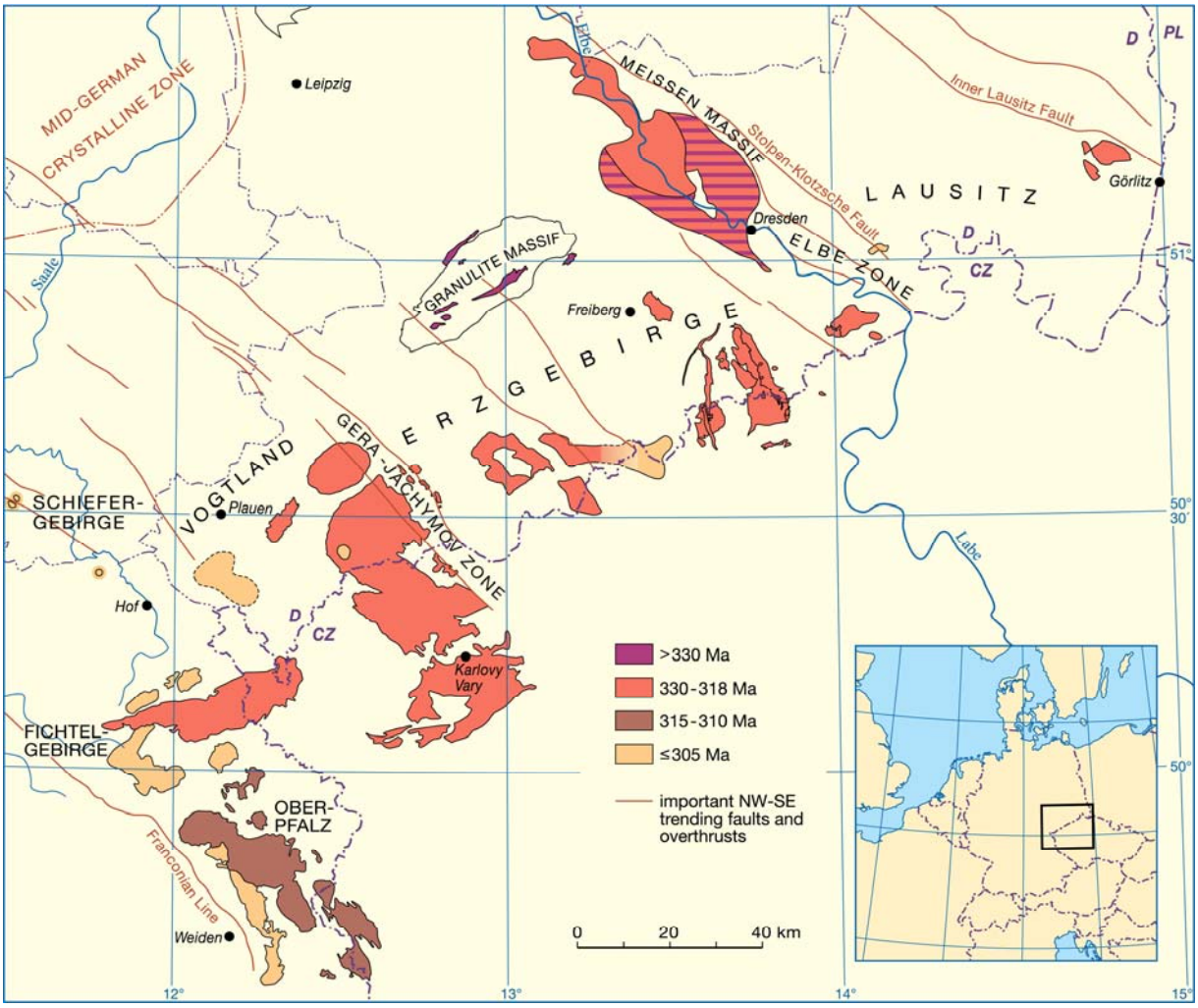
MID-GERMAN CRYSTALLINE ZONE
Leipzig
MEISSEN MASSIF
Stolpen-Klotzsche Fault
Inner Lausitz Fault
D
PL
LAUSITZ
Görlitz
Dresden
ELBE ZONE
CZ
GRANULITE MASSIF
Freiberg
ERZGEBIRGE
Saale
VOGTLAND
GERA-JÁCHYMOV ZONE
SCHIEFER-GEBIRGE
Plauen
Hof
Karlovy Vary
FICHTEL-GEBIRGE
OBER-PFALZ
Franconian Line
Weiden
Labe
>330 Ma
330-318 Ma
315-310 Ma
≤305 Ma
important NW-SE trending faults and overthrusts
0
20
40 km
12°
13°
14°
15°
50°
30'
51°

Figure 7

**Table 1** Composition of uraninite from Königshain

| Grain No. | uraninite 1 | | uraninite 2 | |
|---|---|---|---|---|
| $ThO_2$ | 6.42 | 6.84 | 6.78 | 5.08 |
| $UO_2$ | 79.00 | 77.31 | 82.56 | 78.08 |
| $Y_2O_3$ | 4.18 | 3.84 | 1.94 | 3.85 |
| $La_2O_3$ | 0.00 | 0.00 | 0.00 | 0.04 |
| $Ce_2O_3$ | 0.40 | 0.52 | 0.17 | 0.33 |
| $Pr_2O_3$ | 0.16 | 0.08 | 0.03 | 0.07 |
| $Nd_2O_3$ | 0.54 | 0.85 | 0.11 | 0.78 |
| $Sm_2O_3$ | 0.66 | 0.74 | 0.49 | 0.91 |
| $Gd_2O_3$ | 1.40 | 1.41 | 1.06 | 1.65 |
| $Tb_2O_3$ | 0.29 | 0.37 | 0.17 | 0.33 |
| $Dy_2O_3$ | 1.22 | 1.75 | 0.77 | 2.13 |
| $Ho_2O_3$ | 0.17 | 0.21 | 0.18 | 0.13 |
| $Er_2O_3$ | 0.74 | 0.92 | 0.56 | 1.22 |
| $Yb_2O_3$ | 0.59 | 0.75 | 0.35 | 0.63 |
| $Lu_2O_3$ | 0.13 | 0.12 | 0.28 | 0.05 |
| PbO | 3.71 | 3.58 | 3.83 | 3.72 |
| total | 99.59 | 99.29 | 99.28 | 98.99 |

**Table 2** Th–Pb–U concentrations and single-spot ages of uraninite from Königshain

| Anal. No | $ThO_2$ | PbO | $UO_2$ | age (Ma) | Anal. No | $ThO_2$ | PbO | $UO_2$ | age (Ma) |
|---|---|---|---|---|---|---|---|---|---|
| | **uraninite 1** | | | | | **uraninite 2** | | | |
| I-1 | 6.67 | 3.44 | 74.12 | 327 | 103 | 6.11 | 3.54 | 76.56 | 327 |
| I-2 | 6.33 | 3.59 | 74.79 | 339 | 104 | 5.07 | 3.64 | 79.14 | 327 |
| I-3 | 5.56 | 3.56 | 77.43 | 326 | 105 | 6.48 | 3.76 | 79.22 | 335 |
| I-4 | 6.60 | 3.41 | 73.32 | 328 | 106 | 7.32 | 3.65 | 77.56 | 331 |
| I-5 | 6.36 | 3.43 | 75.05 | 323 | 107 | 6.11 | 3.74 | 79.73 | 332 |
| I-6 | 6.34 | 3.38 | 73.93 | 323 | 108 | 4.48 | 3.49 | 76.46 | 325 |
| I-7 | 6.31 | 3.49 | 78.12 | 316 | 109 | 6.19 | 3.74 | 80.58 | 328 |
| I-8 | 6.40 | 3.42 | 75.55 | 320 | 110 | 6.09 | 3.80 | 80.29 | 335 |
| I-9 | 6.21 | 3.59 | 76.74 | 331 | 111 | 5.35 | 3.67 | 77.53 | 336 |
| 48 | 6.34 | 3.42 | 73.74 | 327 | 112 | 5.25 | 3.67 | 79.49 | 328 |
| 49 | 6.31 | 3.40 | 73.28 | 327 | 113 | 4.75 | 3.61 | 80.30 | 320 |
| 50 | 7.45 | 3.49 | 73.95 | 331 | 32 | 6.54 | 3.11 | 68.30 | 321 |
| 51 | 6.26 | 3.51 | 75.58 | 328 | 33 | 6.31 | 3.47 | 72.11 | 339 |
| 52 | 6.60 | 3.46 | 75.83 | 322 | 34 | 6.02 | 3.43 | 71.79 | 337 |
| 53 | 6.51 | 3.48 | 74.68 | 328 | 35 | 6.09 | 3.37 | 72.28 | 329 |
| 54 | 6.82 | 3.42 | 75.30 | 320 | 36 | 7.09 | 3.25 | 69.34 | 329 |
| 55 | 6.09 | 3.50 | 75.73 | 327 | 37 | 6.65 | 3.22 | 69.13 | 328 |
| 56 | 6.24 | 3.54 | 75.14 | 332 | 38 | 6.29 | 3.31 | 70.01 | 333 |
| 57 | 6.95 | 3.55 | 74.71 | 334 | 39 | 5.35 | 3.18 | 69.34 | 325 |
| 58 | 6.51 | 3.43 | 72.55 | 333 | 40 | 6.39 | 3.32 | 70.72 | 331 |
| 316 | 6.42 | 3.71 | 79.00 | 331 | 41 | 6.87 | 3.52 | 74.53 | 333 |
| 317 | 6.82 | 3.76 | 80.49 | 330 | 42 | 6.08 | 3.48 | 73.85 | 333 |
| 318 | 6.25 | 3.68 | 79.07 | 329 | 385 | 5.26 | 3.76 | 78.55 | 336 |
| 319 | 6.39 | 3.63 | 78.04 | 329 | 386 | 6.58 | 3.72 | 80.40 | 328 |
| 320 | 6.47 | 3.46 | 76.51 | 320 | 387 | 4.98 | 3.65 | 76.55 | 338 |
| 321 | 6.77 | 3.54 | 76.55 | 326 | 388 | 6.05 | 3.75 | 79.68 | 333 |
| 322 | 6.29 | 3.59 | 77.75 | 326 | 389 | 6.99 | 3.74 | 79.94 | 330 |
| 323 | 5.35 | 3.71 | 81.24 | 324 | 326 | 6.02 | 3.68 | 80.55 | 324 |
| 324 | 6.12 | 3.79 | 82.17 | 327 | 327 | 5.63 | 3.78 | 81.82 | 328 |
| 325 | 6.61 | 3.67 | 79.59 | 326 | 328 | 5.94 | 3.67 | 78.99 | 329 |

## Supplementary electronic material

Trace-element composition of sample G101 from Königshain

| Element | ppm |
|---|---|
| Li | 100 |
| Be | 9.0 |
| Sc | 4.8 |
| V | 1 |
| Cr | 6 |
| Co | 0.3 |
| Ni | 0.3 |
| Cu | 1.3 |
| Zn | 29.6 |
| Ga | 20.7 |
| As | 2.8 |
| Rb | 335 |
| Sr | 24.2 |
| Y | 62.3 |
| Zr | 98 |
| Nb | 36 |
| Mo | 0.63 |
| Ag | <20 ppb |
| Cd | 0.02 |
| Sn | 8 |
| Sb | 0.64 |
| Cs | 18.5 |
| Ba | 106 |
| La | 18.6 |
| Ce | 44.7 |
| Pr | 5.73 |
| Nd | 24.0 |
| Sm | 7.25 |
| Eu | 0.13 |
| Gd | 8.00 |
| Tb | 1.55 |
| Dy | 9.50 |
| Ho | 1.91 |
| Er | 5.72 |
| Tm | 0.88 |
| Yb | 6.02 |
| Lu | 0.88 |
| Hf | 5.1 |
| Ta | 3.9 |
| W | 2.6 |
| Au | <0.1 |
| Pb | 42.3 |
| Bi | 0.25 |
| Th | 33.5 |
| U | 15.9 |

**EMPA of uraninite**

Chemical dating using the electron microprobe is not trivial and may, in addition to mineral-specific geological problems, also encounter "technical" problems related to the type of used instrument and the dated mineral. Among the geological problems, the most obvious ones are "inheritance" and open-system behaviour that may result in too old and too young apparent ages, respectively.

In the chemical dating of uraninite, inheritance is a minor problem as the large Pb ion does not readily substitute into the crystal structure of uraninite. Minor Pb incorporation into uraninite, however, has been demonstrated in TIMS work. For instance, Förster (1996) documented Pb inheritance in secondary uranium minerals (including remobilized uraninite) in uranium ores. In this special case, the available Pb had a very radiogenic isotopic composition and there was a significant amount of Pb available for redistribution (from in-situ Pb growth in the precursor uraninite), the inheritance became apparent mainly because of the radiogenic composition of the inherited Pb (even if there have been only a few hundred ppm of Pb inherited), which moved the data away from the discordia to apparent ages higher than the age of the last crystallization. During the crystallization of uraninite in magmatic rocks, however, significantly less Pb is available in the system and many minerals show a higher compatibility for Pb. For chemical dating of uraninite, thus, the initial incorporation of Pb (even if it were at a level of few hundred ppm) is of subordinate importance in comparison with *in-situ* Pb growth. For instance, late Carboniferous uraninite has typically more than 3–3.5 wt% Pb, i.e., overestimating the age by <1% in the worst case. Secondary mobility of Pb, resulting in too young apparent ages, is a larger problem and may be avoided by dating uraninite that has inclusions of galena or is rimmed by galena, which may have derived their Pb from uraninite. Furthermore, concentrating dating efforts on minerals that are entirely hosted by one mineral, the possibility of Pb loss to the surrounding is minimized (see discussion for uraninite in Romer et al. 2007 and for monazite in Montel et al. 2000, Williams et al. 2006). Note, Pb inheritance represents a potential problem for minerals with a higher compatibility for Pb than uraninite and – more importantly – lower *in-situ* Pb growth, as for instance for monazite or xenotime.

There may be type-specific differences among electron microprobes in the sets of WDS crystals available and their wavelength resolution. Depending on the crystal resolution, peaks may be completely resolved on some instruments, whereas there is some peak overlap on other instruments, requiring correction for such interferences. Thus, the export of a measurement protocol that is highly successful on one microprobe may result in problems on another one. Furthermore, a measurement protocol that is perfectly fine for monazite or xenotime may not work for uraninite, as depending on the contrasting chemical composition of these minerals the optimal position of baseline and selected peaks for Th, U, and Pb and the necessary corrections for interferences may differ.

We tested our measurement protocol used for the dating of uraninite by (i) analyzing the same uraninite grains on different micro-probes using different sets of standards and different wavelength for the various elements (optimized for the corresponding instrument) and by (ii) analyzing the same uraninite grains on one micro-probe using different sets of standards and the same wavelengths. The obtained uraninite ages are identical within analytical uncertainties.

Förster B (1996) U/Pb Datierung an Pechblenden der U-Lagerstätte Aue-Niederschlema (Erzgebirge). Ph.D. Thesis, University Giessen, Germany, 212pp + appendices

Montel J-M, Kornprobst J, Vielzeuf D (2000) Preservation of old U–Th–Pb ages in shielded monazite: example from the Beni Bousera Hercynian kinzigites (Morocco). J metamorphic Geol 18:335–342

Romer RL, Thomas R, Stein HJ, Rhede D (2007) Dating multiply overprinted Sn-mineralized granites – examples from the Erzgebirge, Germany. Mineral Deposita 42:337–359

Williams ML, Jercinovic MJ, Goncalves P, Mahan K (2006) Format and philosophy for collecting, compiling, and reporting microprobe monazite ages. Chem Geol 225:1–15

**Standards - Set-1**

Uraninite measurement conditions (15kV,40nA,focussed beam), *full-element analyses*

| | | | STD | counting time-peak (s) | D.L. (ppm) |
|---|---|---|---|---|---|
| 1 | Ca | Ca-Ka | Wollastonite | 20 | 125 |
| 2 | Fe | Fe-Ka | Fe2O3 | 20 | 290 |
| 4 | Al | Al-Ka | Al2O3 | 20 | 70 |
| 5 | Th | Th-Ma | Metal | 100 | 63 |
| 6 | P | P-Ka | YbPO4 | 20 | 145 |
| 7 | La | La-La | LaPO4 | 50 | 555 |
| 8 | Ce | Ce-La | CePO4 | 50 | 460 |
| 9 | Si | Si-Ka | Wollastonite | 20 | 98 |
| 10 | U | U-Mb | Metal | 100 | 95 |
| 11 | Y | Y-La | YPO4 | 30 | 220 |
| 12 | Pr | P-Lb | PrPO4 | 20 | 750 |
| 13 | Nd | Nd-Lb | NdPO4 | 50 | 690 |
| 15 | Pb | Pb-Mb | Vanadinite | 100 | 105 |
| 17 | Gd | Gd-Lb | GdPO4 | 50 | 725 |
| 18 | Sm | Sm-Lb | SmPO4 | 50 | 699 |
| 21 | Dy | Dy-Lb | DyPO4 | 50 | 810 |
| 22 | Tb | Tb-Lb | TbPO4 | 50 | 760 |
| 24 | Er | Er-Lb | ErPO4 | 50 | 940 |
| 25 | Ho | Ho-Lb | HoPO4 | 50 | 860 |
| 26 | Lu | Lu-La | LuPO4 | 50 | 495 |
| 27 | Yb | Yb-La | YbPO4 | 50 | 455 |

D.L. = detection limit.

*Dating:*

Uraninite (15 kV, 40 nA, focused beam)

| | | STD | counting time-peak (s) | D.L. (ppm) |
|---|---|---|---|---|
| Th | Th-Ma | Metal | 100 | 246 |
| U | U-Mb | Metal | 100 | 142 |
| Y | Y-La | YPO4 | 100 | 83 |
| Pb | Pb-Mb | Vanadinite | 100 | 129 |

Uraninite (15 kV, 20 nA, focused beam)

| | | STD | counting time-peak (s) | D.L. (ppm) |
|---|---|---|---|---|
| Th | Th-Ma | Metal | 100 | 359 |
| U | U-Mb | Metal | 100 | 202 |
| Y | Y-La | YPO4 | 100 | 119 |
| Pb | Pb-Ma | Vanadinite | 100 | 122 |

Uraninite (20 kV, 40 nA, spot size 1 μm)

| | | STD | counting time-peak (s) | D.L. (ppm) |
|---|---|---|---|---|
| Th | Th-Ma | Metal | 50 | 177 |
| U | U-Mb | Metal | 50 | 283 |
| Y | Y-La | YPO4 | 50 | 112 |
| Pb | Pb-Ma | Vanadinite | 80 | 77 |

Uraninite (20 kV, 40 nA, focused beam)

| | | STD | counting time-peak (s) | D.L. (ppm) |
|---|---|---|---|---|
| Th | Th-Ma | Metal | 50 | 175 |
| U | U-Mb | Metal | 50 | 309 |
| Y | Y-La | YPO4 | 50 | 112 |
| Pb | Pb-Mb | Vanadinite | 50 | 164 |

**Standards - Set-2**

JXA-8500F
Uraninite (15 kV, 40 nA, spot size 1 μm)

| | | STD | counting time-peak (s) | D.L. (ppm) |
|---|---|---|---|---|
| Th | Th-Ma | Metal-II | 50 | 204 |
| U | U-Mb | UO2 | 50 | 375 |
| Y | Y-La | YAG | 50 | 117 |
| Pb | Pb-Ma | Vanad-II | 80 | 196 |

CAMECA SX100
Uraninite (15kV, 40 nA, spot size 1 μm)

| | | STD | counting time-peak (s) | D.L. (ppm) |
|---|---|---|---|---|
| Th | Th-Ma | Metal-II | 50 | 355 |
| U | U-Mb | UO2 | 50 | 345 |
| Y | Y-La | YAG | 50 | 190 |
| Pb | Pb-Ma | Vanad-II | 80 | 320 |

**Table 3** Re-Os isotopic data for molybdenite from Königshain

| AIRIE Run Number | Sample Description | Re, ppm | $^{187}$Os, ppb | Common Os, ppb | Age, Ma (analytical uncertainty only) | Age, Ma (full uncertainty) |
|---|---|---|---|---|---|---|
| MDID-695 | molybdenite crystals in open space | 3.448 (4) | 11.861 (4) | 0.00 (4) | 327.6 ± 0.4 | 327.6 ± 1.1 |
| MDT-695 | molybdenite crystals in open space | 3.453 (7) | 11.857 (4) | 0.006 (2) | 327.0 ± 0.7 | 327.0 ± 1.3 |

Molybdenite mineral separates created at AIRIE from quarry hand sample; maximum silicate dilution is 10%

Carius tube dissolution and spike equilibration using mixed-double Os spike (Markey et al. 2003); sample weight is 135 mg

Two runs represent single dissolution, sample run on two TIMS mass spectrometers (MDID is NBS single-collector, MDT is Triton multi-collector)

All data corrected for blank (Re and Os concentrations, Os isotopic composition), common Os, and mass fractionation

Re blank = 0.72 ± 0.01 pg, Os blank = 0.730 ± 0.002 pg, and $^{187}$Os/$^{188}$Os blank composition = 0.257 ± 0.001

Double Os spike used to determine common Os and correct for Os mass fractionation; Re mass fractionation accounted for by total evaporation method

Errors are two-sigma and absolute for last decimal place indicated; assumed initial $^{187}$Os/$^{188}$Os = 0.2 ± 0.1

Full uncertainties quoted for ages (last column) include the decay constant uncertainty for $^{187}$Re and propagation of all analytical error